Journal of Solid State Chemistry **153,** 275–281 (2000)
doi:10.1006/jssc.2000.8758, available online at http://www.idealibrary.com on IDEAL®

Powder Neutron Diffraction Studies of $Na_2Ti_2Sb_2O$ and Its Structure–Property Relationships

Tadashi C. Ozawa, Rigo Pantoja, Enos A. Axtell, III, and Susan M. Kauzlarich[1]

Department of Chemistry, University of California, One Shields Avenue, Davis, California 95616

John E. Greedan and Mario Bieringer

Institute for Materials Research, McMaster University, Hamilton, Ontario L8S 4M1, Canada

and

James W. Richardson Jr.

Intense Pulsed Neutron Source, Argonne National Laboratory, IPNS/360, 9700 South Cass Avenue, Argonne, Ilinois 60439-4814

Received January 18, 2000; in revised form May 1, 2000; accepted May 4, 2000; published online July 7, 2000

The structure of $Na_2Ti_2Sb_2O$ has been investigated by temperature-dependent powder neutron diffraction. $Na_2Ti_2Sb_2O$ crystallizes in *I4/mmm* symmetry. The structure of this phase can be viewed as an anti-K_2NiF_4 type where Ti^{3+} ion is located between two oxygen atoms forming a square-planar lattice. Powder neutron diffraction studies of $Na_2Ti_2Sb_2O$ indicate that this compound has a structural distortion in the $[Ti_2Sb_2O]^{2-}$ layer at $T \approx 120$ K. This transition corresponds well to the previously reported anomalous transition temperature of the magnetic susceptibility and electronic resistivity. Several models to explain the data are presented and discussed. © 2000 Academic Press

Key Words: **pnictide–oxide; neutron diffraction; CDW; SDW; layered oxide.**

INTRODUCTION

The structure–property relationship in oxide materials exhibiting anomalous electronic and magnetic properties has attracted much attention. Recent examples include $CuGeO_3$ (1) and $NaTiO_2$ (2, 3). Both $CuGeO_3$ and $NaTiO_2$ exhibit a sharp drop in temperature-dependent magnetic susceptibility. However, the mechanisms responsible for this property are quite different. In the case of $CuGeO_3$, the sharp drop of the magnetic susceptibility is caused by a spin-Peierls transition, that is, a progressive dimerization of an insulating one-dimensional antiferromagnetic spin lattice (4), whereas the magnetic susceptibility drop observed for $NaTiO_2$ is induced by a hexagonal-to-monoclinic structural transition. Other examples are alkali-metal bronzes of tungsten (5, 6) and molybdenum (7–9) oxides. These materials exhibit anomalous transitions in both magnetic susceptibility and electronic resistivity. The origin of the anomalies in these materials is referred to as a charge-density wave (CDW)/spin-density wave (SDW), which is a modulation of charge density or spin density associated with a structural distortion in conducting materials (10). Understanding the structure–property relationship of these types of compounds provides a framework for designing new materials with interesting properties. Recently, we reported an anomaly in the temperature-dependent electronic resistivity and magnetic susceptibility of a layered pnictide–oxide, $Na_2Ti_2Sb_2O$ (11, 12). This compound has a sharp transition in resistivity and magnetic susceptibility at $T_c \approx 120$ K (Fig. 1). The resistivity exhibits metal-to-metal (MM) transition reminiscent of quasi-two-dimensional CDW/SDW materials, concurrent with a sharp drop in the magnetic susceptibility reminiscence of spin-Peierls materials (1, 13). This is the first example of this type of behavior in a layered pnictide–oxide (11, 12, 14–25) or oxy-chalcogenide (26–30) and the report (12) of the properties of $Na_2Ti_2Sb_2O$ has generated much interest (31–34).

This compound crystallizes in tetragonal (*I*4/*mmm*) symmetry and has a layered structure (Fig. 2) resembling a high-T_c superconductor, $La_{2-x}Ba_xCuO_{4-\delta}$ (K_2NiF_4 type) (35). However, $Na_2Ti_2Sb_2O$ is an anti-K_2NiF_4 type, where Ti^{3+} ion is located between oxygen atoms, forming a square-planar layer, $[Ti_{4/2}O]^{4+}$, which is an anticonfiguration to the $[CuO_{4/2}]^{2-}$ layer in high-T_c cuprates (11). Ti^{3+} is also four coordinated by Sb^{3-}, forming a $[Ti_2Sb_2O]^{2-}$ layer where Sb^{3-} is located above and below the center of

[1] To whom correspondence should be addressed.

0022-4596/00 $35.00

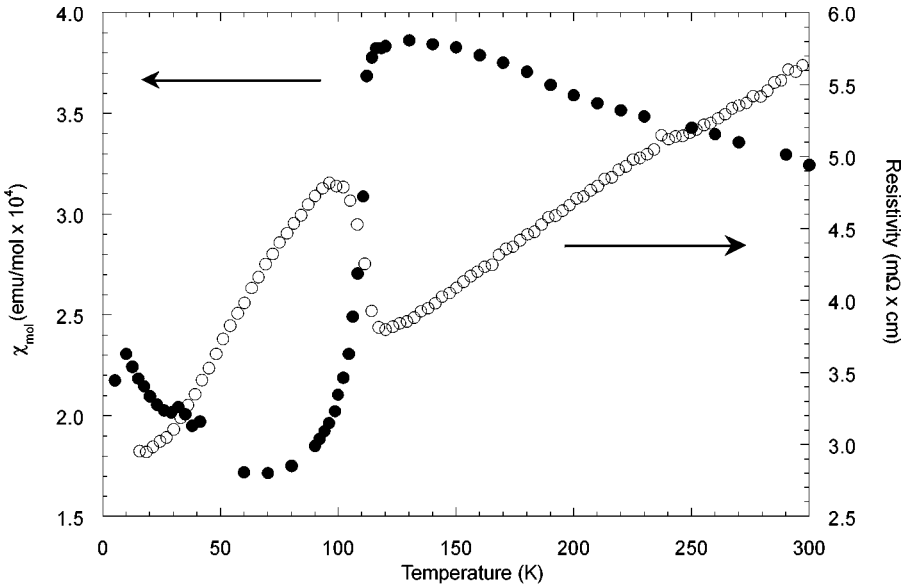

FIG. 1. Temperature-dependent magnetism and electric resistivity of $Na_2Ti_2Sb_2O$ (Adapted from Ref. 12).

the $[Ti_{4/2}O]^{4+}$ square unit. $[Ti_2Sb_2O]^{2-}$ layers are stacked in a body-centered manner along the c axis, and those layers are separated by double layers of Na^+. There are only a few examples of layered compounds with anti-$[CuO_2]^{2-}$-type layers; one such example is $Na_{1.9}Cu_2Se_2Cu_2O$ (26). The electronic structure of $Na_2Ti_2Sb_2O$ has been studied by two groups (31, 34) and a structural distortion concomitant with the electronic and magnetic transition is suggested. In this paper, we report the results of temperature-dependent powder neutron diffraction of $Na_2Ti_2Sb_2O$. Based on the experimental results, its structure–property relationship will be discussed.

EXPERIMENTAL PROCEDURES

Sample preparation. Approximately 5 g of $Na_2Ti_2Sb_2O$ was prepared by solid-state sintering of Na_2O (Aldrich, 97%), Ti (Cerac, 99.98%), and Sb (Cerac, 99.999%). Phase purity of each starting material was verified by powder X-ray diffraction. Ti and Sb were found to be phase pure; however, the diffraction pattern of Na_2O showed secondary peaks due to Na_2O_2. To account for this, the stoichiometry was optimized as

$$x\mathrm{Na_2O_2} + (100 - x)\mathrm{Na_2O} + 200\mathrm{Ti} + 200\mathrm{Sb}$$

$$\rightarrow 100\mathrm{Na_2Ti_2Sb_2O} + x\mathrm{O_2},$$

where x was varied from 0 to 10 by the increment of 1. This optimization of the stoichiometry resulted in $x = 5$ yielding the most pure phase. Thus, the samples for the powder neutron diffraction studies were synthesized accordingly:

$$5\mathrm{Na_2O_2} + 95\mathrm{Na_2O} + 200\mathrm{Ti} + 200\mathrm{Sb}$$

$$\rightarrow 100\mathrm{Na_2Ti_2Sb_2O} + 5\mathrm{O_2}.$$

All starting materials were mixed in an agate mortar and pestle and pressed into pellets in an argon-filled drybox. Pellets were sealed in pre-etched Ta tubing and enclosed in a fused silica ampoule under 1/5 atm argon gas. The ampoule was heated at 60°C/h to 1000°C, dwelled there for 24 h, and then cooled to room temperature at the rate of 250°C/h. The resulting product has a gray-black color and retains the original pellet shape. The product purity was checked by powder X-ray diffraction on a Guinier camera utilizing Cu$K\alpha_1$ radiation with NBS silicon as an internal reference. The powder diffraction pattern was compared with the calculated pattern based on the previously published single-crystal crystallographic data (11) and gave excellent agreement in 2θ positions and intensities. No extra peaks were observed.

Spallation source powder neutron diffraction. Temperature-dependent neutron data of $Na_2Ti_2Sb_2O$ were obtained using the general purpose powder diffractometer (GPPD) at the Intense Pulsed Neutron Source (IPNS) at Argonne National Laboratory. Approximately 5 g of sample was loaded into a vanadium tube and sealed with an indium gasket under a helium atmosphere. The temperature of the sample was controlled by a helium closed-cycle cryostat. The diffraction patterns were acquired at 19

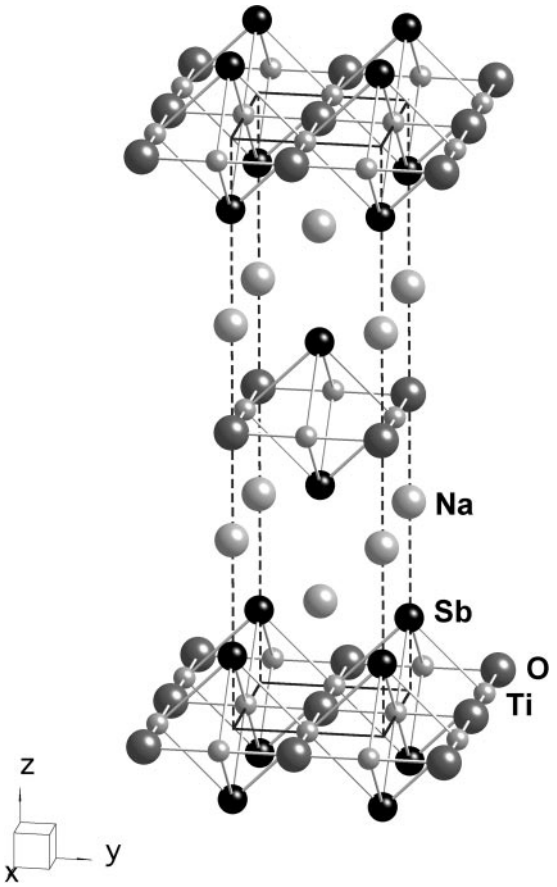

FIG. 2. Crystal structure of $Na_2Ti_2Sb_2O$ showing alternation of $[Ti_2Sb_2O]^{2-}$ layers and double layers of Na^+.

temperatures between 10 and 300 K. These diffraction patterns showed several extra peaks that were not observed in the powder X-ray diffraction of the same sample, suggesting that they originate from scattering of the neutron beam from the experimental setup. Structural information was obtained by Rietveld refinement using the GSAS software package (36).

Reactor source powder neutron diffraction. The magnetic structure was investigated by powder neutron diffraction on the DUALSPEC diffractometer at the Chalk River Laboratories of AECL (Atomic Energy of Canada Limited). Diffraction patterns were acquired at 150 and 15 K using $\lambda = 2.3692$ Å wavelength neutron beam. The sample was enclosed in a vanadium tube sealed with an indium gasket. The temperature was controlled by a helium closed-cycle cryostat.

RESULTS AND DISCUSSION

Room temperature structural information obtained by Rietveld refinement of powder neutron diffraction data agreed well with results from previously published single-crystal data (11). The observed, calculated, and difference profiles of the Rietveld refinement of diffraction data from the GPPD at 150 K are shown in Fig. 3. Extra peaks resulting from diffraction of the experimental setup were removed. Only one of these regions included a diffraction peak from $Na_2Ti_2Sb_2O$, which is of low intensity. The refined parameters are summarized in Table 1, and the plot of lattice parameters as a function of temperature is shown in Fig. 4. The Rietveld refinement of the temperature-dependent neutron powder diffraction data from the GPPD indicates a structure distortion at $T \approx 120$ K, corresponding to the transition in the temperature-dependent magnetic susceptibility and electrical resistivity. Upon cooling, the lattice parameter c decreases linearly at the rate of 0.000439 Å/K above T_c, then it deviates from the linearity, and decreases faster below T_c. In contrast, the lattice parameter a does not exhibit linearity, even above the T_c, and the rate of its decrease is faster than that of the c parameter. a/c shows an effect similar to that of a, but is less pronounced (Fig. 4 inset). No significant change in the fractional coordinate of each atom in the unit cell was found, whereas there is a rapid expansion in the a parameter between 105 and 120 K. A fascinating feature in the lattice parameters vs temperature plot is that the lattice parameter a plummets at T_c, resembling that of CMR manganites (37, 38). The minimum of the plummet is at $T = 120$ K, which corresponds well with the T_c of the temperature-dependent magnetic susceptibility and electrical resistivity. Locally, there is an expansion of the Ti–O bond in this region as the temperature decreases. The a parameter does not change significantly below $T \approx 105$ K. These results indicate that the anomalous behavior of resistivity and magnetism in $Na_2Ti_2Sb_2O$ is coupled with a structural distortion.

There are several theory papers published on the electronic structure and magnetic spin interaction of $Na_2Ti_2Sb_2O$ with the aim of providing insight into the physical property anomaly (31–34). A nested Fermi surface, which develops CDW/SDW instability, has been suggested to account for the anomaly of resistivity (34) and magnetism (31). Also, it is suggested that direct Ti ⋯ Ti d-orbital interaction contributes to this CDW/SDW instability, although the Ti ⋯ Ti distance (~ 2.94 Å) is longer than that in other phases, such as the Ti metal and Ti_2O_3 (31–34, 39). In addition, the possibility of Ti ⋯ Ti second neighbor interaction has been proposed (31, 32). Furthermore, band structure calculation (31) shows that the O p state energy should be lower than that of common transition-metal oxides due to its four coordination with highly charged ions (Ti^{3+}), and the Sb p state energy is more likely to be near the Ti d state energy than the O p state energy (31, 33). Thus, coupling through Ti–Sb–Ti rather than Ti–O–Ti should dominate.

Based on the theoretical argument concerning the O p and Sb p energy levels, the relationship between the

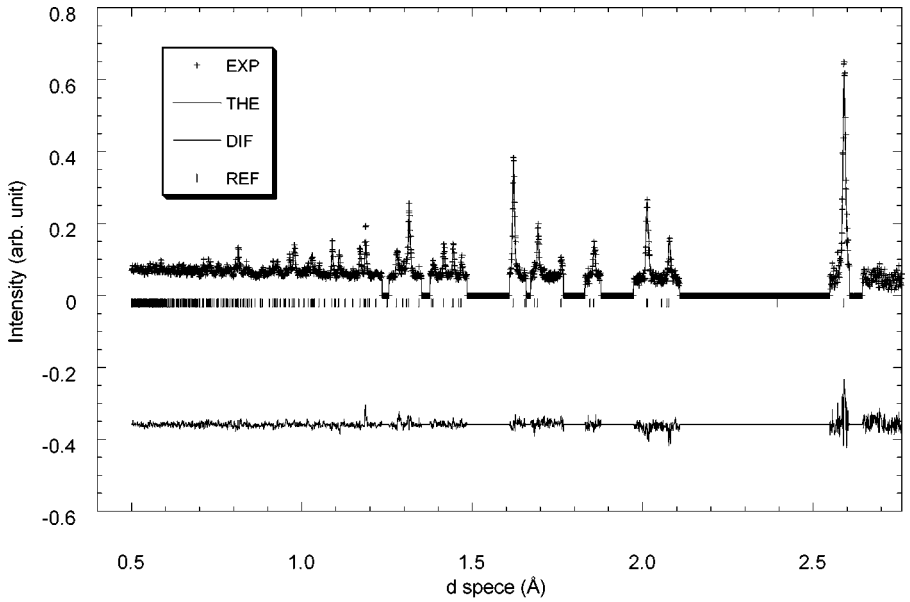

FIG. 3. Rietveld plot of powder neutron diffraction from GPPD ($\pm 148^\circ$ detector bank). Experimental and calculated diffraction patterns are represented by (+) and a solid line, respectively. Their difference is indicated below. Lower tick marks represent calculated reflection positions.

expansion of the *a* parameter and the anomaly in the electrical resistivity can be explained in terms of $^2T_{2g}$ Jahn–Teller–like distortion. Figure 5 shows the molecular orbital diagram of the Ti octahedral unit (*x* and *y* axes in the Sb–Ti–Sb plane but staggered and the *z* axis along O–Ti–O) in $Na_2Ti_2Sb_2O$. The oxidation state of Ti is 3 + , and thus it has a d^1 electronic configuration. In this model, we assume that a d^1 electron of the Ti^{3+} resides in doubly degenerate orbitals: d_{xz} and d_{yz}, and this assumption agrees with the theoretical model used by Singh *et al.* (32). This differs from our initial ideas presented where the d^1 electron resides in a nondegenerate d_{xy} orbital (*x* and *y* axes along Sb–Ti–Sb;

TABLE 1A
Rietveld Refinement Results of Powder Neutron Diffraction Data from GPPD

	300 K	242 K	200 K	150 K	140 K	130 K	120 K	115 K	110 K	105 K
$a = b$ (Å)	4.15567(9)	4.15303(12)	4.15122(9)	4.14966(9)	4.14929(9)	4.14921(10)	4.14892(9)	4.14895(9)	4.14916(9)	4.14937(9)
c (Å)	16.5824(6)	16.5597(8)	16.5404(6)	16.5173(6)	16.5126(6)	16.5067(6)	16.5034(6)	16.5009(6)	16.4968(5)	16.4925(5)
Volume (Å^3)	286.371(13)	285.616(18)	285.035(13)	284.421(13)	284.292(13)	284.178(14)	284.083(13)	284.043(13)	284.002(13)	283.955(13)
R_{wp}	0.0753	0.1072	0.0820	0.0834	0.0836	0.0907	0.0833	0.0838	0.0830	0.0839
R_p	0.0492	0.0754	0.0555	0.0564	0.0563	0.0637	0.0559	0.0563	0.0563	0.0567
χ^2	4.320	1.699	3.306	3.417	3.447	2.444	3.417	3.449	3.360	3.452
Na (0 0 z)	0.31946(31)	0.3188(4)	0.31923(28)	0.31888(27)	0.31894(27)	0.31911(29)	0.31896(26)	0.31915(25)	0.31819(25)	0.31879(25)
Na $U_i/U_e \times 100$	1.95	1.86	1.49	1.29	1.24	0.98	1.08	1.12	1.14	1.20
Na U_{11}	2.00(13)	1.51(16)	1.60(12)	1.33(11)	1.28(11)	1.13(14)	1.21(11)	1.32(11)	1.27(10)	1.36(10)
Na U_{33}	1.85(27)	2.6(4)	1.27(25)	1.20(23)	1.15(23)	0.69(25)	0.83(22)	0.72(21)	0.88(20)	0.88(20)
Ti $U_i/U_e \times 100$	1.14	1.14	0.82	0.79	0.74	0.80	0.53	0.63	0.63	0.57
Ti U_{11}	0.93(18)	0.94(24)	0.97(18)	0.99(17)	0.82(17)	1.18(20)	0.54(15)	0.82(16)	0.72(15)	0.66(15)
Ti U_{33}	2.49(25)	2.06(33)	1.48(21)	1.38(20)	1.40(19)	1.22(22)	1.06(18)	1.06(18)	1.15(17)	1.06(17)
Sb (0 0 z)	0.12116(15)	0.12149(21)	0.12159(15)	0.12169(15)	0.12171(14)	0.12181(16)	0.12164(14)	0.12169(14)	0.12166(14)	0.12181(14)
Sb $U_i/U_e \times 100$	1.46	1.49	1.09	1.00	0.97	0.79	0.83	0.86	0.91	0.89
Sb U_{11}	1.62(10)	1.76(14)	1.40(10)	1.29(9)	1.31(9)	1.15(11)	1.12(9)	1.13(9)	1.27(8)	1.17(8)
Sb U_{33}	1.14(15)	0.94(20)	0.46(13)	0.41(12)	0.29(12)	0.06(13)	0.26(11)	0.32(11)	0.20(11)	0.32(11)
O $U_i/U_e \times 100$	1.37	1.34	0.91	0.83	0.74	0.88	0.58	0.62	0.59	0.62
O U_{11}	0.59(11)	0.65(16)	0.49(11)	0.55(11)	0.57(11)	0.67(16)	0.41(11)	0.35(10)	0.35(10)	0.39(10)
O U_{33}	2.92(24)	2.70(32)	1.75(20)	1.38(19)	1.08(18)	1.30(21)	0.93(17)	1.14(18)	1.07(17)	1.08(17)

TABLE 1B

	100 K	95 K	90 K	85 K	80 K	70 K	50 K	20 K	10 K
$a = b$ (Å)	4.14935(9)	4.14938(8)	4.14931(8)	4.14943(9)	4.14939(8)	4.14926(8)	4.14931(10)	4.14936(9)	4.14940(9)
c (Å)	16.4891(5)	16.4865(5)	16.4840(5)	16.4813(6)	16.4800(5)	16.4765(5)	16.4706(6)	16.4674(6)	16.4671(6)
Volume (Å^3)	283.895(13)	283.854(12)	283.802(12)	283.772(13)	283.743(12)	283.665(12)	283.569(14)	283.523(13)	283.522(13)
R_{wp}	0.0850	0.0832	0.0847	0.0908	0.0834	0.0829	0.1006	0.0923	0.0921
R_p	0.0569	0.0560	0.0576	0.0629	0.0556	0.557	0.0704	0.0643	0.0632
χ^2	3.544	3.350	3.505	2.447	3.375	3.347	1.992	2.391	2.503
Na (0 0 z)	0.31905(25)	0.31917(23)	0.31880(25)	0.31873(26)	0.31896(24)	0.31881(23)	0.31924(26)	0.31906(24)	0.31904(24)
Na $U_i/U_e \times 100$	1.08	1.00	0.95	0.96	0.95	0.89	0.76	0.69	0.79
Na U_{11}	1.16(10)	1.18(10)	1.06(9)	1.10(10)	1.07(9)	0.99(9)	0.94(11)	0.85(10)	0.95(10)
Na U_{33}	0.93(20)	0.64(19)	0.71(20)	0.68(20)	0.96(19)	0.68(18)	0.38(21)	0.35(20)	0.48(20)
Ti $U_i/U_e \times 100$	0.67	0.65	0.59	0.55	0.51	0.52	0.55	0.46	0.42
Ti U_{11}	0.93(16)	0.79(15)	0.75(15)	0.73(16)	0.72(15)	0.77(15)	0.88(18)	0.62(16)	0.66(16)
Ti U_{33}	1.09(18)	1.15(17)	1.02(17)	0.92(18)	0.80(16)	0.79(16)	0.78(19)	0.76(18)	0.61(17)
Sb (0 0 z)	0.12172(14)	0.12177(14)	0.12185(14)	0.12182(15)	0.12198(13)	0.12177(13)	0.12185(16)	0.12165(14)	0.12180(14)
Sb $U_i/U_e \times 100$	0.88	0.81	0.74	0.70	0.69	0.72	0.61	0.53	0.58
Sb U_{11}	1.19(8)	1.13(8)	1.01(8)	1.00(8)	0.98(7)	1.05(7)	0.87(9)	0.77(9)	0.82(9)
Sb U_{33}	0.25(11)	0.17(10)	0.19(11)	0.10(11)	0.11(10)	0.04(10)	0.08(12)	0.05(11)	0.11(11)
O U_i/U_e100	0.65	0.60	0.51	0.54	0.50	0.50	0.41	0.40	0.42
O U_{11}	0.45(10)	0.41(10)	0.36(10)	0.39(10)	0.31(10)	0.28(9)	0.28(11)	0.20(11)	0.15(10)
O U_{33}	1.03(17)	0.98(16)	0.83(16)	0.83(17)	0.89(16)	0.93(16)	0.68(18)	0.80(17)	0.96(17)

z axis along Ti–O) (12). Previously, we coupled bond length with bond strength and presumed that the crystal field of the O^{2-} would have a larger effect than Sb^{3-}. Based on the theoretical calculations (31), this is not the case and the Sb^{3-} is expected to provide a stronger splitting, thereby producing the orbital splitting diagram shown in Fig. 6b. Below the T_c, expansion in the a direction induces the relative increase in Ti–O (apical) distance while there is no significant change in Ti–Sb (equatorial) distance. Thus, d_{xz}, d_{yz}, and d_z^2 are more stabilized with respect to d_{xy} and $d_{x^2-y^2}$ (Fig. 6c). This change in the orbital configuration stabilizes the electronic structure of $Na_2Ti_2Sb_2O$ because the energy of an electron-occupied level becomes lower after the distortion. Furthermore, since there is an increase in the

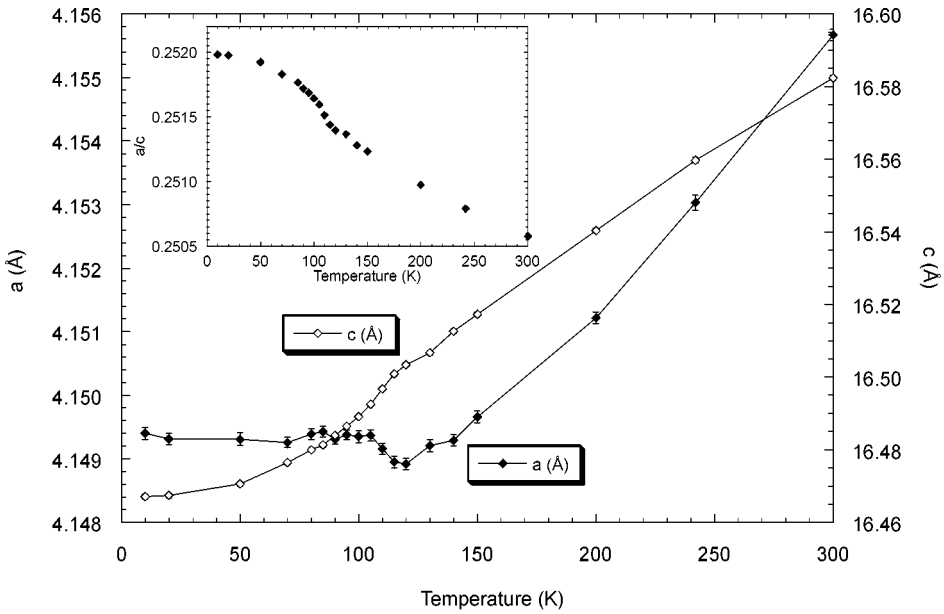

FIG. 4. Lattice parameters a and c as a function of temperature acquired from Rietveld refinement of powder neutron diffraction data from GPPD. a/c vs T plotted in inset.

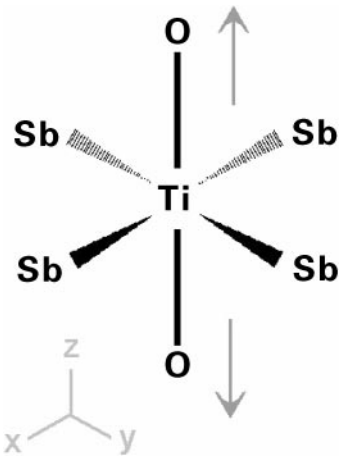

FIG. 5. Octahedral coordination of Ti with arrows showing the local distortion along O–Ti–O axis around the $T \approx 120$ K.

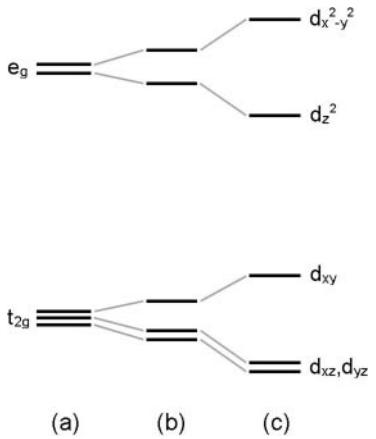

FIG. 6. Crystal field splitting of (a) ordinary undistorted octahedral and $Na_2Ti_2Sb_2O$ (b) above T_c and (c) below T_c.

Ti ⋯ Ti distance, there is also a decrease in the Ti ⋯ Ti metallic interaction through the d_{xz} and d_{yz} orbitals. Thus, the d^1 electron is more localized on Ti^{3+} ion and this results in higher resistivity. This model also correlates well with the Ti ⋯ Ti direct interaction as contributing to the CDW/SDW instability as suggested in theory papers (31–34). Here, the electrical transition is not metal-to-insulator (MI) but MM. This is because the structural distortion yields only partial opening of the band gap as in the case of quasi-two-dimensional metals (6).

The diffraction patterns from a reactor source neutron powder diffractometer, DUALSPEC, at $T = 150$ and 15 K and their difference curve are shown in Fig. 7. There is no superlattice reflection from magnetic ordering or crystal symmetry breakdown that can be discerned from the difference curve. Our initial hypothesis of the origin of the anomalous transition in temperature-dependent magnetism was that of a spin-Peierls transition (4, 40, 41) because of the similarity between the magnetism of $Na_2Ti_2Sb_2O$ and the one-dimensional spin-Peierls material, $CuGeO_3$ (1). $Na_2Ti_2Sb_2O$ can be structurally related to $CuGeO_3$ having a Ti–Sb ribbon chain reminiscent of the Cu–O chain in $CuGeO_3$. In the case of $CuGeO_3$, the Cu-O chain dimerizes alternatively, and this is the cause of the spin-Peierls coup-

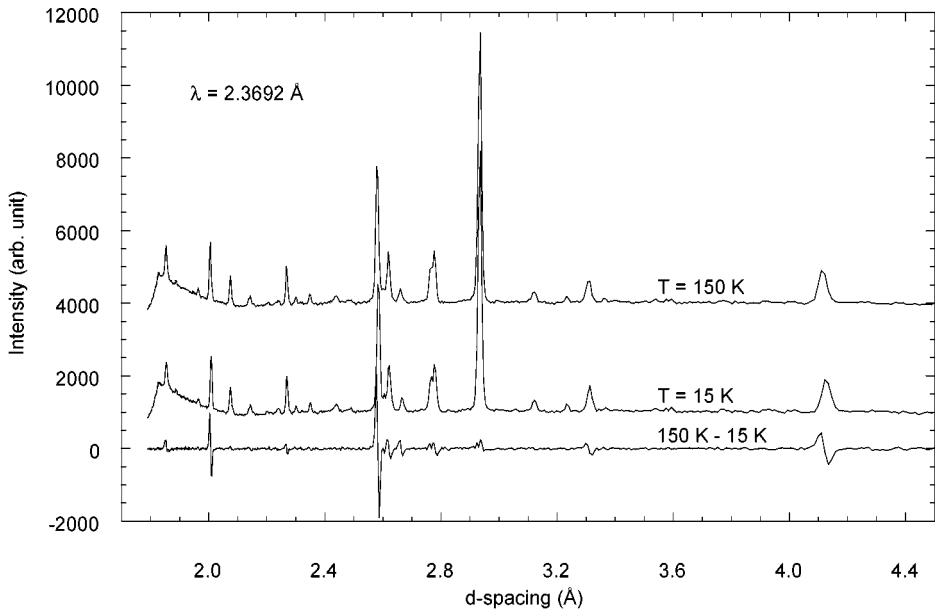

FIG. 7. Powder neutron diffraction profiles at 150 and 15 K along with their difference obtained from DUALSPEC, indicating no significant supercell reflections.

ling. We hypothesized a similar structure modulation in $Na_2Ti_2Sb_2O$ in a two-dimensional manner, corresponding to the theoretically expected Ti–Sb–Ti coupling (31, 33). However, refinement of diffraction data does not support this model. Since resistivity indicates the metallic nature of the compound below T_c, a more likely origin of the anomalous magnetic behavior is CDW/SDW (12, 31, 34). CDW/SDW materials, such as molybdenum oxide bronzes (7–9), show a similar type of transition in temperature-dependent magnetic susceptibility that is also caused by a periodic structure modulation. In these types of compounds the periodic structure modulation cannot be discerned in powder neutron experiments. The results to date suggest either that $Na_2Ti_2Sb_2O$ is a new CDW/SDW compound or that it has a different or more sophisticated magnetism than CDW/SDW systems. Additional experiments such as electron, synchrotron X-ray, and neutron scattering on a single-crystal sample are required to provide insight into the detailed mechanism of the $Na_2Ti_2Sb_2O$ anomaly.

ACKNOWLEDGMENTS

We thank Robert N. Shelton for the use of the powder X-ray diffractometer. Useful discussions with Warren E. Pickett and Rajiv R. P. Singh are gratefully acknowledged. The work was funded by NSF DMR-9803074 and the Natural Sciences and Engineering Research Council of Canada. We also thank I. Swainson and R. Donaberger for assistance with the neutron diffraction experiments at the DUALSPEC facility, which is operated by the Neutron Program for Materials Research of the National Research Council of Canada. This work has also benefited from the use of the Intense Pulsed Neutron Source at Argonne National Laboratory. This facility is funded by the U.S. Department of Energy, BES-Materials Science, under Contract W-31-109-Eng-38.

REFERENCES

1. M. Hase, I. Terasaki, and K. Uchinokura, *Phys. Rev. Lett.* **70,** 3651 (1993).
2. S. J. Clark, A. J. Fowkes, A. Harrison, R. M. Ibberson, and M. J. Rosseinsky, *Chem. Mater.* **10,** 372 (1998).
3. K. Takeda, K. Miyake, K. Takeda, and K. Hirakawa, *J. Phys. Soc. Jpn.* **61,** 2156 (1992).
4. I. S. Jacobs, J. W. Bray, J. Hart, H. R., L. V. Interrante, J. S. Kasper, G. D. Watkins, D. E. Prober, and J. C. Bonner, *Phys. Rev. B* **14,** 3036 (1976).
5. M. Greenblatt, *Int. J. Modern Phys. B* **7,** 3937 (1993).
6. M. Greenblatt, *Acc. Chem. Res.* **29,** 219 (1996).
7. R. D. Buder, J., J. Dumas, J. Marcus, J. Mereier, and C. Schlenker, *J. Phys. Lett.* **43,** L (1982).
8. M. Greenblatt, K. V. Ramanujachary, and W. H. McCarroll, *J. Solid State Chem.* **59,** 149 (1985).
9. M. Greenblatt, *Chem. Rev.* **88,** 31 (1988).
10. P. A. Cox, "The Electronic Structure and Chemistry of Solids." Oxford Univ. Press, Oxford, 1987.
11. A. Adam and H.-U.Z. Schuster, *Anorg. Allg. Chem.* **584,** 150 (1990).
12. E. A. Axtell, III, T. Ozawa, S. M. Kauzlarich, and R. R. P. Singh, *J. Solid State Chem.* **134,** 423 (1997).
13. M. Weiden, R. Hauptmann, C. Geibel, F. Steglich, M. Fischer, P. Lemmens, and G. Güntherodt, *Z. Phys. B* **103,** 1 (1997).
14. T. Ozawa, M. M. Olmstead, S. L. Brock, S. M. Kauzlarich, and D. M. Young, *Chem. Mater.* **10,** 392 (1998).
15. E. Brechtel, G. Cordier, and H. Schäfer, *Z. Naturforsch. B* **30,** 777 (1979).
16. N. T. Stetson and S. M. Kauzlarich *Inorg. Chem.* **30,** 392 (1991).
17. S. L. Brock and S. M. Kauzlarich, *Inorg. Chem.* **33,** 2491 (1994).
18. S. L. Brock and S. M. Kauzlarich, *Chem. Tech.* **25,** 18 (1995).
19. S. L. Brock and S. M. Kauzlarich, *Comments Inorg. Chem.* **17,** 213 (1995).
20. S. L. Brock and S. M. Kauzlarich, *J. Alloys. Compd.* **241,** 82 (1996).
21. S. L. Brock, N. P. Raju, J. E. Greedan, and S. M. Kauzlarich, *J. Alloys Compd.* **237,** 9 (1996).
22. A. T. Nientiedt, W. Jeitschko, P. G. Pollmeier, and M. Brylak, *Z. Naturforsch.* **52b,** 560 (1997).
23. A. T. Nientiedt and W. Jeitschko, *Inorg. Chem.* **37,** 386 (1998).
24. S. L. Brock, H. Hope, and S. M. Kauzlarich, *Inorg. Chem.* **33,** 405 (1994).
25. R. J. Cava, H. W. Zandbergen, J. J. Krajewski, T. Siegrist, H. Y. Hwang, and B. Batlogg, *J. Solid State Chem.* **129,** 250 (1997).
26. Y. Park, D. C. DeGroot, J. L. Schinder, C. R. Kannewurf, and M. G. Kanatzidis, *Chem. Mater.* **5,** 8 (1993).
27. W. J. Zhu, and P. H. Hor, *J. Solid State Chem.* **130,** 319 (1997).
28. W. J. Zhu, P. H. Hor, A. J. Jacobson, G. Crisci, T. A. Albright, S. H. Wang, and T. Vogt, *J. Am. Chem. Soc.* **119,** 12398 (1997).
29. W. J. Zhu and P. H. Hor, *Inorg. Chem.* **36,** 3576 (1997).
30. W. J. Zhu and P. H. Hor, *J. Solid State Chem.* **134,** 128 (1997).
31. W. E. Pickett, *Phys. Rev. B* **58,** 4335 (1998).
32. R. R. P. Singh, O. A. Starykh, and P. J. Freitas, *J. Appl. Phys.* **83,** 7387 (1998).
33. S. K. Pati, R R. P. Singh, and D. I. Khomskii, *Phys. Rev. Lett.* **81,** 5406 (1998).
34. F. Fabrizi de Biani, P. Alemany, and E. Canadell, *Inorg. Chem.* **37,** 5807 (1998).
35. J. G. Bednorz, K. A. Müller, *Z. Phys. B* **64,** 189 (1986).
36. A. C. Larson and R. B. Von Dreele, "LANSCE, MS-H805." Los Alamos National Laboratory, Los Alamos, NM, 1990.
37. D. N. Argyriou, T. M. Kelley, J. F. Mitchell, R. A. Robinson, R. Osborn, S. Rosenkranz, R. I. Sheldon, and J. D. Jorgensen, *J. Appl. Phys.* **83,** 6374 (1998).
38. D. N. Argyriou, J. F. Mitchell, J. D. Jorgensen, J. B. Goodenough, P. G. Radaelli, D. E. Cox, and H. N. Bordallo, *Aust. J. Phys.* **52,** 279 (1999).
39. J. B. Goodenough, *Phys. Rev.* **117,** 1442 (1960).
40. R. E. Peierls, "Quantum Theory of Solids." Clarendon, Oxford, 1955.
41. H. J. Schulz, in "Low-Dimensional Conductors and Superconductors" D. Jérome, C., L. G., Eds.), p. 95. Plenum, New York, 1987.